Bioactive Materials 26 (2023) 88–101

Contents lists available at ScienceDirect

Bioactive Materials

journal homepage: www.keaipublishing.com/en/journals/bioactive-materials

Sustained release of magnesium and zinc ions synergistically accelerates wound healing

Fan Yang [a,b], Yijia Xue [a,b], Feilong Wang [a,b], Danni Guo [a,b], Yunjiao He [a,b], Xiao Zhao [a,b], Fanyu Yan [a,b], Yuqian Xu [a,b], Dandan Xia [b,c,**], Yunsong Liu [a,b,*]

[a] Department of Prosthodontics, Peking University Hospital of Stomatology, Beijing, 100081, China
[b] National Center for Stomatology, National Clinical Research Center for Oral Diseases, National Engineering Research Center of Oral Biomaterials and Digital Medical Devices, Beijing Key Laboratory of Digital Stomatology, Research Center of Engineering and Technology for Computerized Dentistry Ministry of Health, NMPA Key Laboratory for Dental Materials, Beijing, 100081, China
[c] Department of Dental Materials, Peking University Hospital of Stomatology, Beijing, 100081, China

ARTICLE INFO

Keywords:
Biodegradable magnesium
Biodegradable zinc
GelMA hydrogel
Skin wound healing
STAT3 signaling pathway

ABSTRACT

Skin wounds are a major medical challenge that threaten human health. Functional hydrogel dressings demonstrate great potential to promote wound healing. In this study, magnesium (Mg) and zinc (Zn) are introduced into methacrylate gelatin (GelMA) hydrogel via low-temperature magnetic stirring and photocuring, and their effects on skin wounds and the underlying mechanisms are investigated. Degradation testing confirmed that the GelMA/Mg/Zn hydrogel released magnesium ions (Mg^{2+}) and zinc ions (Zn^{2+}) in a sustained manner. The Mg^{2+} and Zn^{2+} not only enhanced the migration of human skin fibroblasts (HSFs) and human immortalized keratinocytes (HaCats), but also promoted the transformation of HSFs into myofibroblasts and accelerated the production and remodeling of extracellular matrix. Moreover, the GelMA/Mg/Zn hydrogel enhanced the healing of full-thickness skin defects in rats via accelerated collagen deposition, angiogenesis and skin wound re-epithelialization. We also identified the mechanisms through which GelMA/Mg/Zn hydrogel promoted wound healing: the Mg^{2+} promoted Zn^{2+} entry into HSFs and increased the concentration of Zn^{2+} in HSFs, which effectively induced HSFs to differentiate into myofibroblasts by activating the STAT3 signaling pathway. The synergistic effect of Mg^{2+} and Zn^{2+} promoted wound healing. In conclusion, our study provides a promising strategy for skin wounds regeneration.

1. Introduction

The skin acts as a barrier against many pathogens and chemical toxins, helps prevent against mechanical injury, and protects the vital organs of the body from invasion [1–4]. Skin damage often leads to the formation of scar tissue and the loss of skin accessories [5,6]. Extensive soft tissue damage exceeding the body's natural regenerative capacity can be life-threatening and may have serious financial consequences [2]. Skin wounds often require dressing, which provides a temporary barrier against infection, prevents dryness, and facilitates the migration and growth of skin cells and subsequent infiltration and integration of host tissues. Thus, wound dressing has a significant impact on wound healing [7–10].

Wound dressing is key for soft tissue healing [11]. Bandages, pads, and gauzes are widely used traditional wound dressings that protect the wound to a certain extent, and absorb exudates such as pus and blood in the wound. However, they also have many disadvantages. For example, they are uncomfortable, the low water content does not provide a moist healing environment, and they are unsuitable for loading biological active substances to promote wound healing [7,12]. Moreover, because of their nonbiodegradable nature, traditional dressings such as sponges, gauze, and bandages absorb blood and form solid clots that attach to

Peer review under responsibility of KeAi Communications Co., Ltd.
* Corresponding author. Department of Prosthodontics, Peking University School and Hospital of Stomatology, No.22, Zhongguancun South Avenue, Haidian District, Beijing, 100081, China.
** Corresponding author. Department of Dental Materials, Peking University School and Hospital of Stomatology, No.22, Zhongguancun South Avenue, Haidian District, Beijing, 100081, China.
E-mail addresses: dandanxia@pku.edu.cn (D. Xia), liuyunsong@hsc.pku.edu.cn (Y. Liu).

https://doi.org/10.1016/j.bioactmat.2023.02.019
Received 17 January 2023; Received in revised form 16 February 2023; Accepted 17 February 2023

wounds, leading to secondary bleeding and pain. In addition, delayed vascularization is an important cause of delayed wound healing. Restoring an adequate blood supply to treat large-scale skin defects is a major scientific and clinical challenge [13]. Therefore, it is very important to develop biodegradable wound dressings that can effectively promote angiogenesis and accelerate the transformation of fibroblasts into myofibroblasts for skin.

Hydrogels are attractive new dressings due to their unique combination of biological and physical properties [14–19]. Methacrylate gelatin (GelMA) hydrogel not only has good biocompatibility, but also has adjustable mechanical, swelling, degradation, and biological properties, making it an excellent wound dressing for different body parts and wound types [20,21]. In addition, GelMA hydrogel is an excellent carrier of bioactive substances [22,23].

Zinc (Zn) is an important coenzyme in tissue repair and a component of many proteins [24–27]. It also plays an important role in a series of wound healing processes, including coagulation [25], cellular immune regulation [24], epithelial regeneration, and extracellular matrix deposition [28]. In addition, magnesium ions (Mg^{2+}) are closely associated with soft tissue. The concentration of Mg^{2+} affects the migration and adhesion of human skin fibroblasts (HSFs) [29,30]. Magnesium ions can promote angiogenesis [31–34] and zinc ions (Zn^{2+}) transport into rat bone marrow stem cells (rBMSCs) [35]. Recent studies encapsulated Zn salt, ZnO nanoparticles, magnesium (Mg) salt, and Mg–Cu particles in hydrogels (alginate and gelatin hydrogels) to promote wound healing [36–40]. However, there has been no study on the combined application of Zn and Mg metal particles in wound dressings, nor on the application or mechanism of Mg^{2+} and Zn^{2+} in the transformation of fibroblasts into myofibroblasts.

Herein, we designed a GelMA hydrogel loaded with Zn and Mg particles (GelMA/Mg/Zn) for treating skin wounds. In this paper, the morphology, degradation characteristics, ion release behavior, and cytocompatibility of GelMA/Mg/Zn hydrogel were analyzed *in vitro*, and its *in vitro* biological activity and *in vivo* effect on skin wounds were studied. Finally, the possible mechanism whereby GelMA/Mg/Zn hydrogel promotes soft tissue healing was explored.

2. Materials and methods

2.1. Preparation of hydrogels

GelMA hydrogel and 0.25% (w/v) LAP solution were mixed in the proportion of 5% (w/v) and heated to 60–70 °C to form a homogeneous prepolymer solution of GelMA hydrogel, which was then placed in a suitable mold and photocured with a 405 nm light source to prepare the control GelMA hydrogel. Magnesium and Zn particles were added to the GelMA prepolymer solution in the ratio of 2.5% (w/v) and mixed at 10 °C. The same procedure was followed to prepare GelMA/Mg and GelMA/Zn hydrogels. Similarly, Mg and Zn particles were added to the GelMA prepolymer solution at the ratio of 1.25% (w/v) to form the GelMA/Mg/Zn hydrogel.

2.2. Characterization of hydrogels

After freeze-drying, the four kinds of hydrogels were sputtered with a thin layer of gold. A scanning electron microscope (SEM; EVO 18; Zeiss, Oberkochen, Germany) operating at an accelerating voltage of 10 kV was used to examine the surface morphology. An energy dispersion spectrometer (INCA X-ACT; Oxford Instruments, Abingdon, UK) was used for elemental analysis of the hydrogels. Scanning electron microscopy (SEM) images were analyzed using Nano Measurer 1.2 software; the diameter of the Zn and Mg particles was measured, and a particle size distribution diagram was generated using Fiji software (ver. 1.49, open source).

2.3. Zn^{2+} and Mg^{2+} release behavior

Wafer-shaped hydrogel specimens (15 mm in diameter and 1.5 mm in height) were immersed in phosphate-buffered saline (PBS) at 37 °C. The ratio of sample weight to solution volume was 0.1 g/mL. The Zn^{2+} and Mg^{2+} concentrations in the extracts of the samples at 0, 3, 6, 12, 24, 48, 72, and 120 h were determined by inductively coupled plasma-optical emission spectrometry (ICP-OES; iCAP6300; Thermo Fisher Scientific, Waltham, MA, USA). The pH value of the PBS at a specific time was measured using a pH meter.

2.4. Mechanical properties

Mechanical properties of hydrogels were analyzed under compression conditions. Each set comprised five cylindrical specimens (11.5 mm in diameter and 8 mm in height). The four hydrogels were placed on the experimental platform of a universal testing machine (Z020; Zwick-Roell, Ulm, Germany) and compressed at 5 mm/min until the hydrogels broke. The elastic modulus was determined from the data acquired during compression.

2.5. Swelling behavior

The hydrogels were placed in PBS at pH 7.4 and 37 °C. The expanded hydrogel specimen was removed at specific intervals and the surface was wiped to remove excess moisture, weighed, and placed back into the PBS. The process was repeated until constant weight was achieved. The swelling ratio (SR) of the sample was calculated as follows:

$$SR = \frac{(Wt - Wo)}{Wo} \times 100\%$$

where W_0 is the initial weight of the dry gel and Wt refers to the weight of the dry gel at time t.

2.6. Degradation behavior

Wafer-shaped hydrogel specimens (15 mm in diameter and 1.5 mm in height) were prepared and immersed in 0.5 mL of 2 U/mL collagenase type II, which is equivalent to the concentration of collagenase during wound healing [41], and shaken at 80 rpm at 37 °C. The collagenase solution was renewed daily to maintain constant collagenase activity. The hydrogel specimen was removed after 0, 3, 6, 9, 12, 24, and 48 h, the moisture was removed from the surface of the hydrogel, and the weight and morphology were recorded. The weight remaining ratio (%) of the hydrogel was calculated as follows:

$$\text{Weight remaining ratio } (\%) = \frac{Wt}{Wo} \times 100\%$$

where W_t and W_0 are the weight of the remaining and initial hydrogel at time point t, respectively.

2.7. Biocompatibility assessment

The HSFs and human immortalized keratinocytes (HaCats) were purchased from Procell Life Science & Technology Co., Ltd. (Wuhan, China). The cells were cultured with Dulbecco's modified Eagle's medium (Gibco, Grand Island, NY, USA) containing 10% fetal bovine serum and 1% penicillin/streptomycin.

The wafer-shaped hydrogel specimens were placed in 24-well culture plates, and HSF cells were inoculated on the hydrogel surface at a density of 2×10^4 cells/well and cultured for 2 days. For the live/dead cell staining experiment, the cells were washed three times with PBS and incubated with 2 μM calcein-AM and 8 μM propidium iodide (Live/Dead Viability/Cytotoxicity Assay for Animal Cells; KeyGen Biotech Corp., Ltd., Jiangsu, China) at room temperature for 45 min. The cells were

then washed three times with PBS, and observed and photographed using a fluorescence microscope (BX53; Olympus, Tokyo, Japan). For the cell attachment test, after washing the hydrogel surface three times with PBS, the cells were immobilized with 4% paraformaldehyde at room temperature for 45 min, followed by infiltration with 0.1% Triton X-100 for 10 min. The cells were washed three times with PBS, and then stained with 5 μg/mL FITC-conjugated phalloidin for 50 min and 4′,6-diamidino-2-phenylindole (Sigma, St. Louis, MO, USA) for 15 min. Then, the cells were observed and photographed using a confocal laser scanning microscope (CLSM; LSM 710; Zeiss).

For the cell proliferation experiment, HSFs and HaCats were inoculated into 24-well plates at a density of 1×10^4 cells/well and cultured with extracts of the four hydrogels. Cells were counted using the Cell Counting Kit-8 (CCK-8; Beijing Aoqing Biotechnology Co., Ltd., Beijing, China) after 0, 1, 2, 3, 4, 5, 6, and 7 days of culture. Optical density at 450 nm (OD450) was measured with a microplate reader.

2.8. Scratch assay

When the fusion rate of HSFs and HaCats reached 90%, a cell scratch was prepared using the tip of a 200 μL pipette, and the shed cells were washed with PBS. Then, the four hydrogel-derived extracts were added to the well, cultured at 37 °C, and observed and photographed at 0, 12, and 24 h using an inverted light microscope. Cell migration images were analyzed using Fiji software. The cell migration ratio was obtained using the following equation:

$$\text{Cell migration ratio } (\%) = \frac{\text{Ao} - \text{At}}{\text{Ao}} \times 100\%$$

where A_0 and A_t are the scratched areas before and after addition of the extract, respectively [42].

2.9. Transwell assay

A Transwell assay was performed to investigate the effect of hydrogels on the migration of HSFs and HaCats. The cells were inoculated into the upper chamber of 12-well Transwell plates (aperture: 8 μm; Corning, NY, USA) and serum-starved for 24 h in 500 μL serum-free medium. The lower chamber was filled with the four kinds of hydrogel extract and cultured at 37 °C at 5% CO_2 for 24 h. After 24 h, the upper chambers were removed and the cells at the top were gently removed using a cotton swab. The cells were fixed with 4% paraformaldehyde at 37 °C for 30 min and then washed three times with PBS. Finally, cells were stained with 5% crystal violet solution. Representative images of each group were taken using an inverted microscope.

2.10. Quantitative real-time PCR (RT-PCR)

Human skin fibroblasts were cultured in the hydrogel-derived extracts for 1 day to evaluate the effect of hydrogel on the expression of α-SMA, and cultured for 2 days to evaluate the effect of hydrogel on the expression of COL1α1, COL3α1, MMP1, MMP9, EGF, FGF2, and FN1. TRIzol reagent (Invitrogen, Carlsbad, CA, USA) was used to extract total RNA from cells. A NanoDrop 8000 spectrophotometer (Thermo Fisher Scientific) was used to determine the purity and concentration of total RNA. Total RNA was reverse-transcribed into cDNA using the PrimeScript RT kit (Takara, Tokyo, Japan). RT-PCR was performed using the QuantStudio3 RT-PCR System (Applied Biosystems, Foster City, CA, USA) and SYBR Green Master Mix (Roche Applied Science, Mannheim, Germany). The primer sequences of human genome GAPDH, α-SMA, COL1α1, COL3α1, MMP1, MMP9, EGF, FGF2, and FN1 are shown in Table S1.

2.11. Intracellular zinc and magnesium ion concentrations

Human skin fibroblasts were cultured with the four hydrogel-derived extracts for 2 days. The cells were digested by trypsin and counted. After centrifugation, cell precipitate was obtained and nitrated with 2% HNO_3 (80 °C, 2 h). The Zn^{2+} and Mg^{2+} contents in the HSF cells were determined by inductively coupled plasma-mass spectrometry (ICP-MS; ELANDRC-e; PerkinElmer, Waltham, MA, USA). Total potassium (K^+) was used as internal reference for the Mg^{2+} and Zn^{2+} measurements; the relative ratios of Mg^{2+} and Zn^{2+} to K^+ were used in the data analysis.

2.12. Evaluation of the effectiveness of hydrogels in promoting wound healing in vivo

Animal experiments were approved by the Animal Research Committee, Peking University Health Science Center (LA 2019019). Twenty male Sprague–Dawley rats weighing 250–300 g at 6–8 weeks were used in the study. The rats were anesthetized by intraperitoneal injection of pentobarbital sodium at 50 mg/kg. Under aseptic conditions, four round full-thickness skin wounds, each with a diameter of 1.5 cm, were established on the back of rats (n = 6). The control (Ctrl; no treatment), GelMA, GelMA/Mg, GelMA/Zn, and GelMA/Mg/Zn were randomly treated with a breathable dressing (Tegaderm film; 3 M, St. Paul, MN, USA). The size of the wound was observed daily and images were taken with a digital camera at fixed focal length on days 0, 3, 5, 7, 9, 11, and 14. Then, the size of the wound was quantified using Fiji image analysis software, and the wound reduction rate was calculated as follows:

$$\text{Wound reduction rate } (\%) = \frac{\text{Ao} - \text{At}}{\text{Ao}} \times 100\%$$

where A_0 is the initial wound area and A_t is the wound area at time point t after injury.

The rats were sacrificed by overdose of anesthetic on days 7 and 14 after operation. The intact tissue of the wound and surrounding parts was excised and fixed with 10% formalin. Then, the samples were dehydrated in an ethanol gradient and embedded in paraffin. After sectioning, the sections were stained with hematoxylin–eosin (H&E) and Masson dyes for histological observation. Immunohistochemical (IHC) staining was performed on the sections to reveal the progress of angiogenesis during wound healing. Such staining of vascular endothelial cell marker CD31 (Sigma-Aldrich, St. Louis, MO, USA) showed regenerated arterioles and capillaries.

After the rats were sacrificed on day 14 after operation, full-thickness skin samples with dimensions of 4×2 cm^2 were prepared, which included the wound area and intact tissue from the wound and surrounding parts. In the tensile strength test, the sample was installed in a fixture with clamp separation of 2 cm and stretched at a crosshead speed of 5 mm/min until fracture. The elastic modulus was obtained using the universal testing machine's bundled software.

2.13. RNA sequencing and bioinformatics analysis

Human skin fibroblasts were cultured in the hydrogel-derived extracts of the four hydrogels for 2 days and total RNA was isolated using TRIzol reagent (Invitrogen) according to the manufacturer's instructions. Three replicates of each sample were sequenced. Transcriptome RNA sequencing was performed by Novogene Biotechnology Co., Ltd. (Beijing, China). Reads containing adapter or ploy-Nb reads, and low-quality reads, were removed to ensure clean, high-quality data for subsequent analysis. DEGSeq2 software (ver. 1.20.0) was used for differential gene expression analysis. A corrected p-value of 0.05 and absolute fold change of 2 were set as the thresholds for significantly differential expression. The clusterProfiler R package (ver. 3.8.1) was used to analyze differentially expressed genes in Kyoto Encyclopedia of Genes and Genomes (KEGG) pathways, to identify important

mechanisms.

2.14. Western blotting

Human skin fibroblasts washed with PBS were lysed in radioimmunoprecipitation assay (RIPA) buffer supplemented with 1% phosphatase inhibitor (Roche Applied Science) and 2% protease inhibitor cocktail (Roche Applied Science). After collecting the cell lysate and centrifuging at 14,000 rpm at 4 °C for 30 min, the supernatant was transferred to a new tube and the protein concentration was determined using a BCA protein analysis kit (Thermo Fisher Scientific). Total protein of each sample was subjected to 10% sodium dodecyl sulfate-polyacrylamide gel electrophoresis (SDS-PAGE). After electrophoresis, the proteins were transferred to a polyvinylidene fluoride membrane (Millipore, Billerica, MA, USA). The membrane was incubated overnight with specific primary antibodies COL1 (Proteintech, Chicago, IL, USA), α-SMA (Proteintech), STAT3 (Huaxingbochuang, Beijing, China), P-STAT3 (Huaxingbochuang), or GAPDH (Cell Signaling Technology, Beverly, MA, USA) at 4 °C after sealing with 10% nonfat milk. The membrane was then incubated with goat anti-rabbit IgG (Abcam, Cambridge, UK) at room temperature. Finally, visualized immunoreactive protein bands were detected using an enhanced chemiluminescence kit (CWBIO, Beijing, China).

2.15. Statistical analysis

The results are expressed as mean ± standard deviation (SD). Comparison of more than two groups was conducted by one-way analysis of variance (ANOVA) using SPSS 22.0 software (SPSS Inc., Chicago, IL, USA). A significance level of 5% was used for all analyses.

3. Results

3.1. Preparation and characterization of GelMA/Mg/Zn hydrogel

We prepared biodegradable GelMA/Mg/Zn, which can release Zn^{2+}

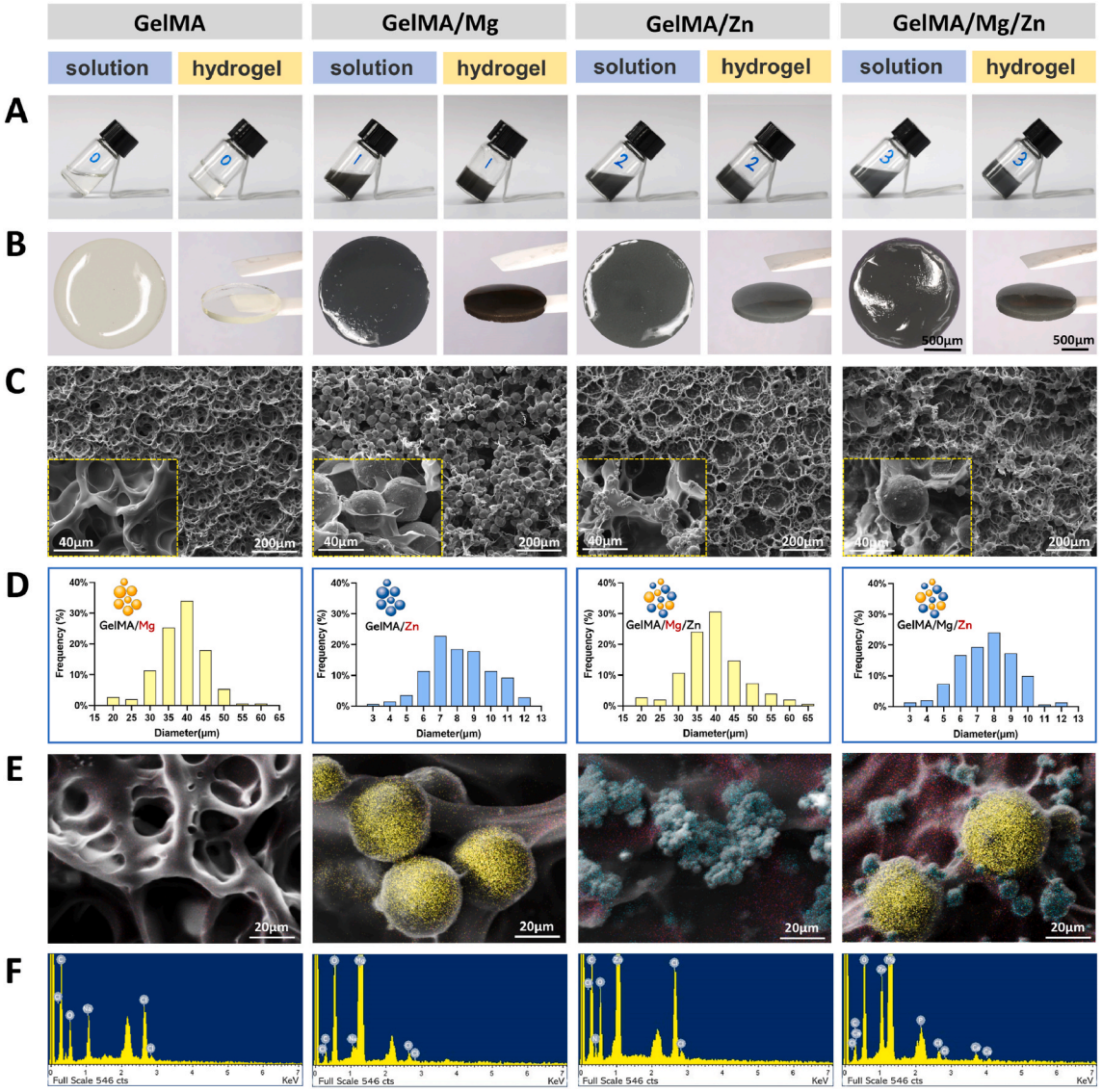

Fig. 1. Morphology and characterization of GelMA/Mg/Zn. (A) GelMA, GelMA/Mg, GelMA/Zn, and GelMA/Mg/Zn solutions before and after 405 nm light treatment. (B) Macro-morphologies of the four types of wafer-shaped hydrogels. (C) Typical scanning electron microscopy (SEM) images of hydrogel cross-sections. Inset at the lower left shows high-resolution SEM results. (D) Diameter distribution of Mg and Zn particles of GelMA/Mg, GelMA/Zn, and GelMA/Mg/Zn. (E, F) Energy-dispersive spectrometry maps and spectra of the four types of hydrogels; yellow, cyan, red, blue, and magenta correspond to elemental Mg, Zn, O, C, and Cl, respectively.

and Mg^{2+} and achieve excellent biological activity, to promote skin regeneration as follows. First, the 5% blank GelMA was prepared as the matrix of the hydrogels and control group. Then, 2.5% Zn, 2.5% Mg, and 1.25% Zn and 1.25% Mg particles were added to the blank GelMA, and a homogeneous hydrogel solution was prepared by a low-temperature magnetic stirring method (Fig. 1A). Subsequent photocuring under 405 nm light provided the GelMA/Mg, GelMA/Zn, and GelMA/Mg/Zn hydrogels (Fig. 1A). GelMA/Mg/Zn was expected to promote wound angiogenesis, and accelerate connective tissue and epithelial regeneration, via release of Zn^{2+} and Mg^{2+}. Photographs of the blank GelMA, GelMA/Mg, GelMA/Zn, and GelMA/Mg/Zn are presented in Fig. 1B. The Zn and Mg particles were evenly dispersed in GelMA, and GelMA/Mg/Zn appeared gray due to the presence of Zn and Mg particles (Fig. 1B). Scanning electron microscopy images (Fig. 1C) confirmed that the four hydrogels had continuous porous structures with pore sizes of 15–100 μm, which are suitable for skin regeneration in adult mammals (20–125 μm) [43]. Moreover, Zn and Mg particles were uniformly distributed in the GelMA hydrogel. Analysis of the SEM images using Fiji software provided the particle size distributions of the metal particles in GelMA/Mg, GelMA/Zn, and GelMA/Mg/Zn (Fig. 1D). Energy-dispersive spectrometry maps (Fig. 1E) and spectra (Fig. 1F) also confirmed the successful incorporation of Zn and Mg particles into GelMA.

To simulate the process of wound healing, GelMA, GelMA/Mg, GelMA/Zn, and GelMA/Mg/Zn were cultured in 2 U/mL type II collagenase solution to evaluate the degradation effect [41]. Fig. 2A and B shows that GelMA was completely degraded after 9 h. The addition of Zn and Mg particles reduced the degradation rate of GelMA, and GelMA/Mg remained on the wound bed for a longer period of time. The degradation rate of the four hydrogels followed the order: GelMA > GelMA/Zn > GelMA/Mg/Zn > GelMA/Mg. This trend suggests that the degradation rate of GelMA/Mg/Zn can be changed by adjusting the size and proportion of Zn and Mg particles to suit different wound sites and wound types. The swelling performance of a hydrogel affects its ability to absorb wound exudate as a wound dressing. We further characterized the swelling rate of the hydrogels (Fig. 2C); the addition of Zn particles did not affect the swelling property of GelMA. The addition of Mg particles increased the swelling rate of GelMA, which may be due to hydrogen generated during the degradation of Mg particles, resulting in more pores in GelMA/Mg.

Release of Zn^{2+} and Mg^{2+} from hydrogels greatly affected the biological activity of the hydrogels. We soaked GelMA, GelMA/Mg, GelMA/Zn, and GelMA/Mg/Zn in PBS at pH 7.4 to characterize their ion release ability. During the first 12 h, the Mg^{2+} release of GelMA/Mg and GelMA/Mg/Zn rapidly increased, and then slowly increased to 284.07 ± 12.79 and 218.96 ± 12.34 μmol/L, respectively (Fig. 2D). The Zn^{2+} release of GelMA/Zn increased to 7.52 ± 0.40 μmol/L during the first 3 days, and the Zn^{2+} release of GelMA/Mg/Zn slowly increased to 1.92 ± 0.29 μmol/L during the first 5 days (Fig. 2E). During the soaking process, we measured the pH value of the PBS in which the hydrogels were soaked. Fig. 2F shows that addition of Mg and Zn particles increased the pH of GelMA to 10.65 and 8.31, respectively. The pH of GelMA/Mg/Zn was also higher than that of GelMA, which eventually stabilized around 10.28. Fig. 2G presents the elastic modulus of the four kinds of hydrogels. The elastic modulus of the GelMA/Mg/Zn hydrogel was 0.042 ± 0.0085 MPa, which was significantly higher than that of the GelMA hydrogel. This result shows that the addition of Zn and Mg particles can overcome the disadvantages of low stiffness and easy breakage of the 5% GelMA hydrogel, which is important for clinical application.

3.2. Biocompatibility assessment of GelMA/Mg/Zn hydrogel

The ability of cells to attach, spread, and grow on hydrogels is critical to wound healing. Fig. 3A shows live/dead staining images of HSFs after 2 days of coculture with the four hydrogels. The proportion of dead cells

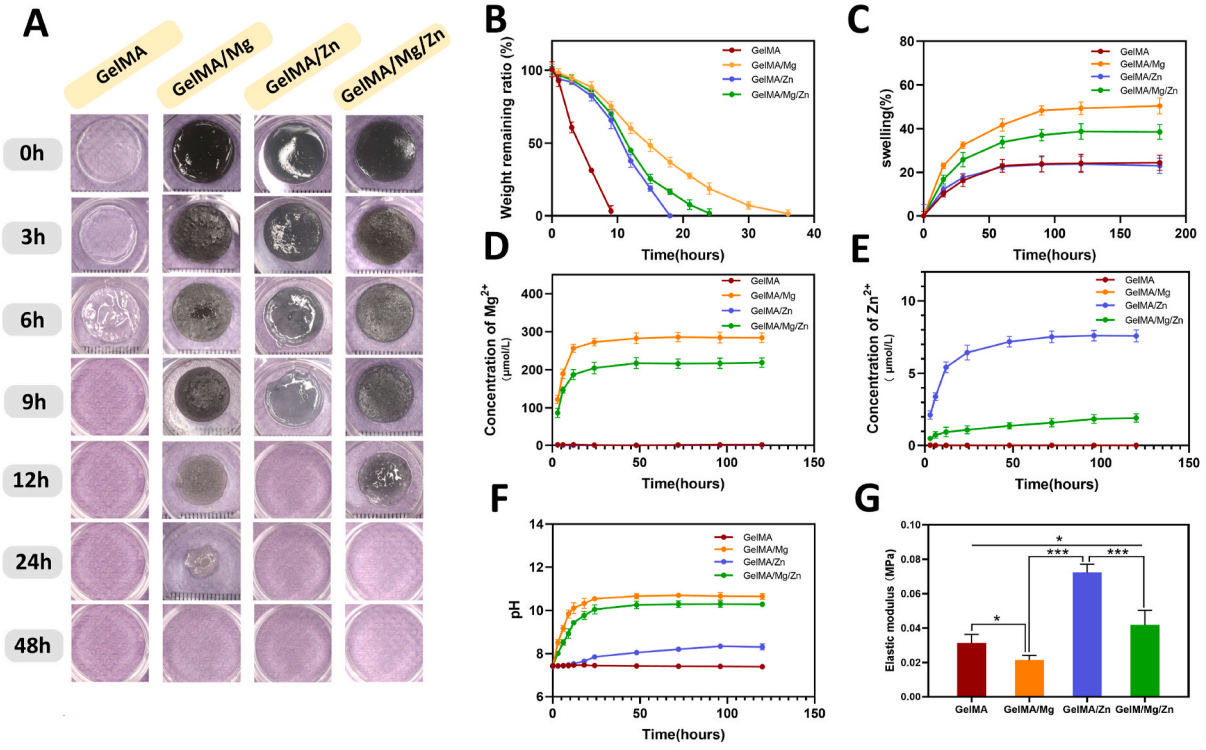

Fig. 2. *In vitro* degradation behavior, immersion test results, and mechanical properties of hydrogels. (A) Representative photos of morphological changes occurring during *in vitro* degradation. (B) Weight remaining ratio during degradation of GelMA, GelMA/Mg, GelMA/Zn, and GelMA/Mg/Zn. (C) Swelling curve of hydrogels soaked in phosphate-buffered saline (PBS) at pH 7.4 and 37 °C. (D, E) Cumulative release of Mg^{2+} and Zn^{2+} from GelMA, GelMA/Mg, GelMA/Zn, and GelMA/Mg/Zn in PBS at pH 7.4. (F) pH values of GelMA, GelMA/Mg, GelMA/Zn, and GelMA/Mg/Zn in PBS of pH 7.4. (G) Quantitative analysis of the elastic modulus of hydrogels. $^{*}p < 0.05$, $^{***}p < 0.001$.

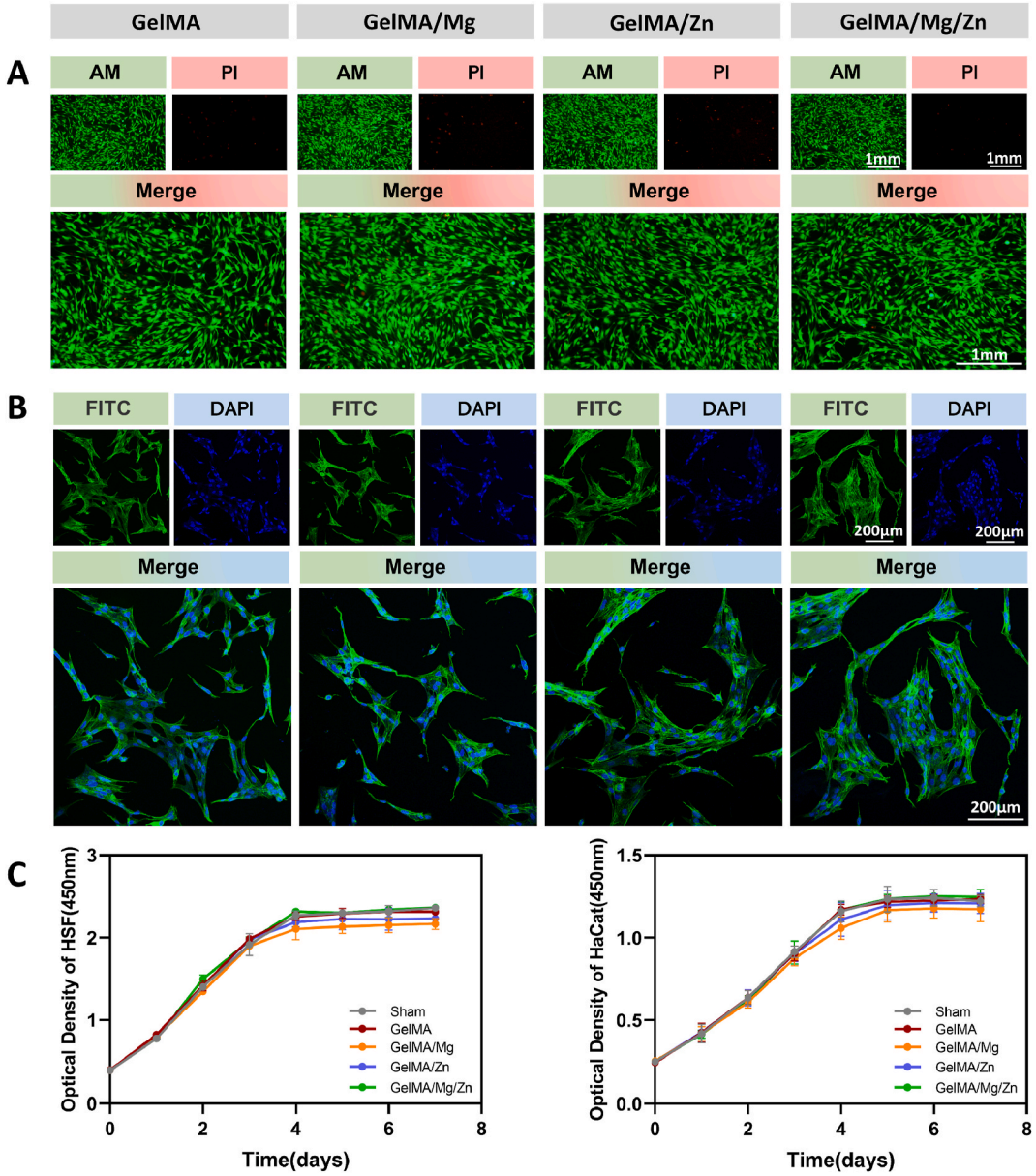

Fig. 3. Biocompatibility assessment. (A) Live/dead cell staining. The red cells correspond to dead cells and the green ones to live cells. (B) Attachment of human skin fibroblasts to GelMA, GelMA/Mg, GelMA/Zn, GelMA/Mg/Zn observed by laser confocal microscopy. (C) Cell proliferation values for each group, obtained using the Cell Counting Kit-8 on days 1, 2, 3, 4, 5, 6, and 7.

(marked in red) on the hydrogel surface in the GelMA/Mg and GelMA/Zn groups was about 9.3% and 5.9%, respectively, i.e., slightly higher than in the GelMA group, while the number of dead cells in the GelMA/Zn and GelMA/Mg/Zn groups was very low and similar to that in the GelMA group. Fig. 3B shows CLSM images of HSFs cocultured with the four hydrogels for 2 days. There were fewer pseudopodia and poor elongation on the surface of GelMA/Mg, which was consistent with the results of the live/dead staining observations. However, on GelMA/Mg/Zn, the cells grew flat and diffused freely, and there were abundant "artificial feet". The HSFs and HaCats were cultured with the four hydrogel-derived extracts, and cell viability was detected by the CCK-8 assay (Fig. 3C). The OD450 of the five groups increased with increasing cell culture time, but the OD450 growth rate of the GelMA/Mg and GelMA/Zn group was slightly lower than that of the other four groups. The results showed the biocompatibility of GelMA/Mg/Zn was better than that of GelMA/Mg and GelMA/Zn.

3.3. Evaluation of the biological effect of GelMA/Mg/Zn hydrogel in vitro

Migration of keratinocytes and fibroblasts plays a crucial role in wound re-epithelialization and closure. The ability of the four hydrogel-derived extracts to promote cell migration was studied by cell scratch and Transwell assays. To ensure that cell migration was not caused by cell proliferation, we treated the cells with serum starvation 24 h before the scratch assay to reduce cell proliferation. The results of the cell scratch and Transwell assays both suggested that the migration ability of HSFs cells was enhanced after treatment of the four hydrogel-derived extracts (Fig. 4A), among which the GelMA/Mg/Zn extract displayed the strongest migration-promoting effect. The cell scratch assay of HaCats showed the same trend, i.e., the four hydrogels promoted migration, with the GelMA/Mg/Zn hydrogel having the greatest effect (Fig. 4C). Quantitative analysis of the cell scratch assay showed that the scratch healing rate of HSFs and HaCats reached 81.14 ± 4.50% and 95.68 ± 2.82%, respectively, after treatment with GelMA/Mg/Zn

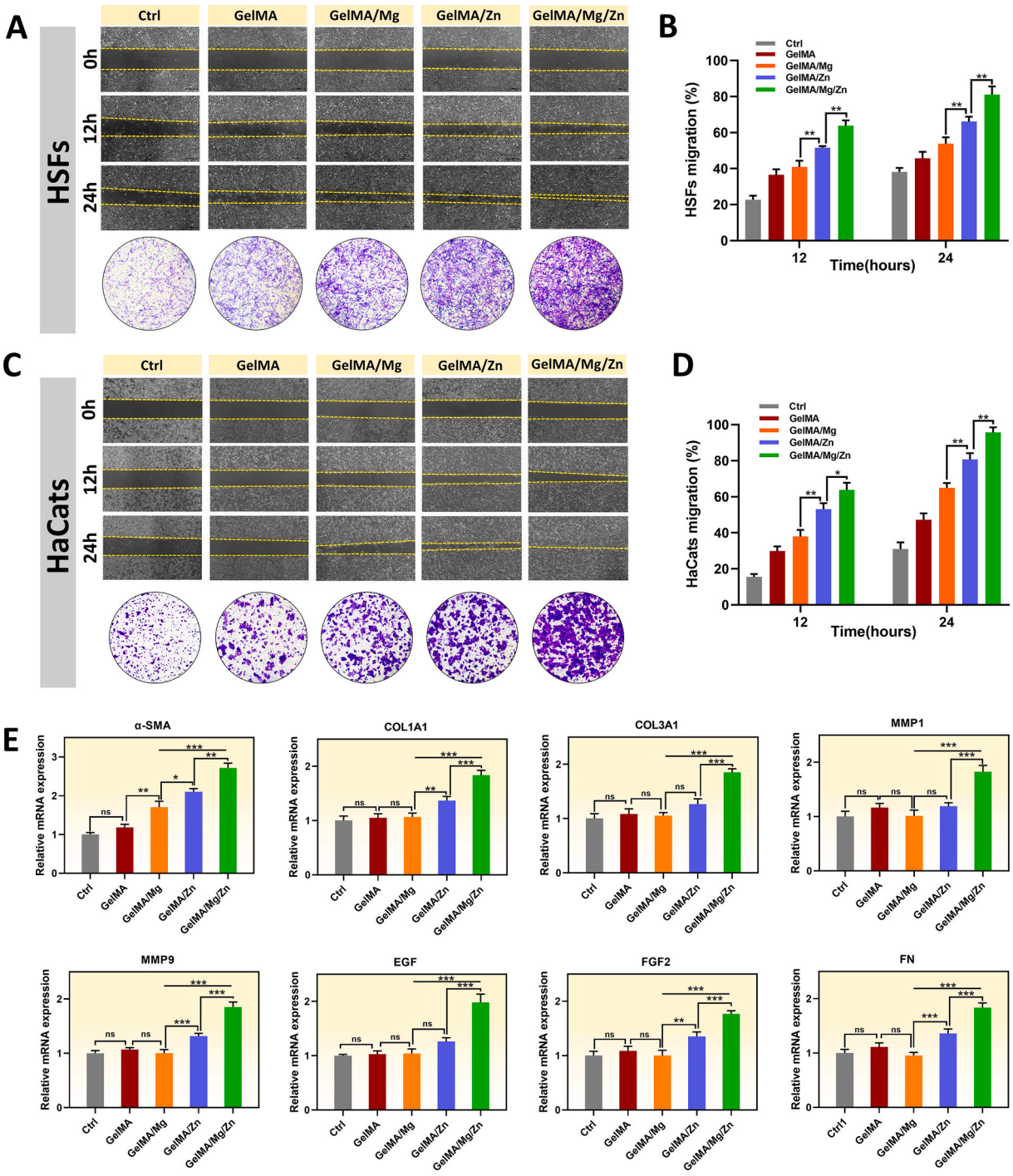

Fig. 4. Migration testing and the expression of wound healing-related RNA of human skin fibroblasts (HSFs) and human immortalized keratinocytes (HaCats). (A, C) Morphological details of the scratch and Transwell assays of HSFs and HaCats after treatment with hydrogel leach liquor at 0, 12, and 24 h. (B, D) Quantitative analysis of the migration area of HSFs and HaCats in the cell scratch assay. (E) The expression levels of α-SMA, COL1A1, COL3A1, MMP1, MMP9, EGF, FGF2, and FN in cultured HSFs after treatment with proliferation medium and the four hydrogel-derived extracts for 24–28 h were determined by RT-qPCR. Data are shown as the mean ± standard deviation (n = 3). $*p < 0.05$, $**p < 0.01$, $***p < 0.001$, ns: not significant.

extract for 24 h (Fig. 4B, D). To further verify the role of Zn^{2+} and Mg^{2+} in cell migration, the scratch assays of HSFs were performed again using salt solutions of $ZnSO_4$ and $MgCl_2$. The results of cell scratch assay showed that 1 and 10 μmol/L $ZnSO_4$ salt solution best-promoted HSF migration (Fig. S1), and 100 μmol/L, 1 mmol/L $MgCl_2$ solutions promoted HSF migration (Fig. S2). The release of Zn^{2+} and Mg^{2+} from hydrogels was in the effective concentration range verified by the cell scratch assay.

Skin fibroblasts can transform into myofibroblasts, which contract, close wounds and produce proteins including collagen and fibronectin (FN), as well as growth factors, to synthesize and reshape the extracellular matrix, which plays a key role in wound healing [3,44]. To study the effect of the four hydrogels on the transformation of fibroblasts into myofibroblasts, RT-qPCR was used to detect the expression capacity of the myofibroblast landmark gene α-SMA (Fig. 4E). Compared with the Ctrl group, the expression of α-SMA in the GelMA/Mg, GelMA/Zn, and GelMA/Mg/Zn groups was increased, and the expression of α-SMA was most obvious in the GelMA/Mg/Zn group. Subsequent RT-qPCR analysis

showed that the expression levels of collagen genes (COL1A1 and COL3A1), FN, growth factors (VEGF, EGF, and FGF2) and matrix metalloproteinases (MMP1 and MMP9) in the GelMA/Mg/Zn group were significantly increased, indicating that the ability of fibroblasts to synthesize and reshape the extracellular matrix was enhanced after GelMA/Mg/Zn extract treatment (Fig. 4E).

3.4. GelMA/Mg/Zn hydrogel effectively promotes skin regeneration in vivo

The effect of the different hydrogels on skin wound healing was evaluated using the rat full-thickness skin defect model. The wounds were divided into five groups: Ctrl, GelMA, GelMA/Mg, GelMA/Zn, and GelMA/Mg/Zn. Macroscopic images of rat skin wounds were taken at fixed focal lengths on days 0, 3, 5, 7, 9, 11, and 14. Fig. 5A and B shows that, on day 14, the wound healing rate was lowest in the Ctrl and GelMA groups, with larger scabs visible at the wound site, followed by the GelMA/Mg group. The wounds in the GelMA/Mg/Zn group left very small scars; the wounds were almost fully healed. Compared with the Ctrl, GelMA, GelMA/Mg, and GelMA/Zn groups, the skin wounds in the GelMA/Mg/Zn group were smaller at all time points and healed better. On day 14, the wound healing rate of the GelMA/Mg/Zn group was 98.9 ± 1.4% (Fig. 5C). Statistical analysis confirmed that the wound healing rate of the GelMA/Mg/Zn group was significantly higher than that of the other four groups (Fig. 5C), which was consistent with the results of the skin stretching test (Fig. 5D).

To investigate the reconstruction of wound tissue, H&E and Masson staining of the wound and surrounding tissue were performed on days 7 and 14 for histopathological analysis (Fig. 6A and B). After 7 days of treatment, histological sections of the Ctrl and GelMA groups showed inflammatory granulation tissue with a large number of neutrophils. Although the granulation tissue thickness in the GelMA/Mg group was greater than that in the Ctrl and GelMA groups, inflammation remained, especially near the wound surface, suggesting that the biocompatibility of GelMA/Mg on the skin surface might be poor and could easily cause inflammation. Both the GelMA/Zn and GelMA/Mg/Zn groups displayed more new collagen fibers at the wound site on day 7, and the initial epithelialization was completed. The wound healing rate of the GelMA/Mg/Zn group was higher than that of the other groups.

After 14 days of treatment, wound healing was best in the GelMA/Mg/Zn group, followed by the GelMA/Zn group; the wound healing of the Ctrl, GelMA, and GelMA/Mg groups was significantly worse. The wound healing of the GelMA/Mg group was slightly better than that of the Ctrl and GelMA groups; more blood vessels were visible, although mature collagen and skin appendages were not observed. Magnified images of the H&E and Masson staining revealed that, compared with the other three groups, the skin wound in the GelMA/Mg/Zn group had the thickest and most complete epidermal layer; more mature and orderly collagen fibers were observed in the dermis layer (Fig. 6A and B), more hair follicles, sebaceous glands and other skin appendages were visible. These results clearly indicated that GelMA/Mg/Zn effectively promoted wound healing.

According to the Masson staining results, the collagen in wound skin of the Ctrl, GelMA, and GelMA/Mg groups was sparse and disordered.

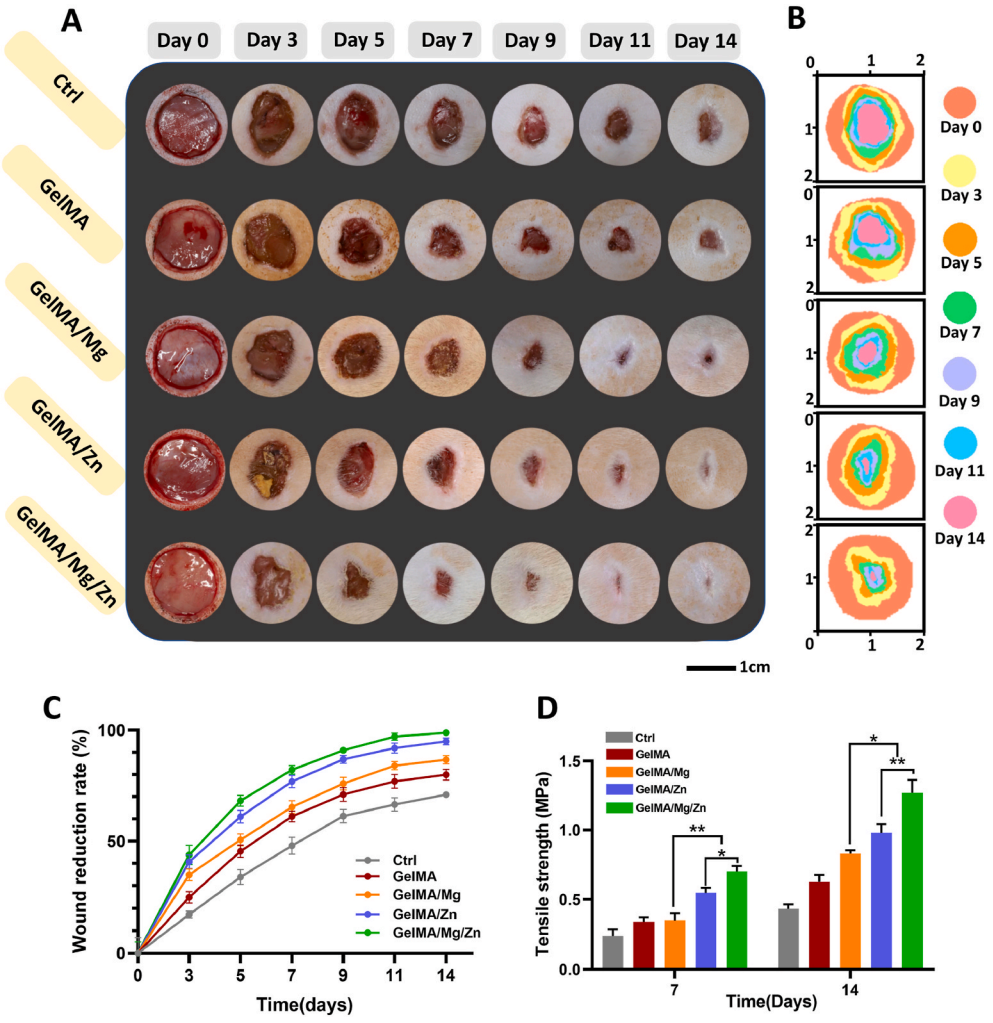

Fig. 5. *In vivo* macro evaluation of wound healing of full-thickness skin defects in rats. (A) Micrographs of full-thickness wounds in rats covered with GelMA, GelMA/Mg, GelMA/Zn, and GelMA/Mg/Zn at days 0, 3, 5, 7, 9, 11, and 14. (B) Schematic illustration of wound morphological changes in the different groups over 14 days. (C) Quantitative comparison of wound area among the five groups. (D) Quantitative comparison of wound tensile strength among the five groups. Data are shown as the mean ± standard deviation (n = 6). $^{*}p < 0.05$, $^{**}p < 0.01$, ns: not significant.

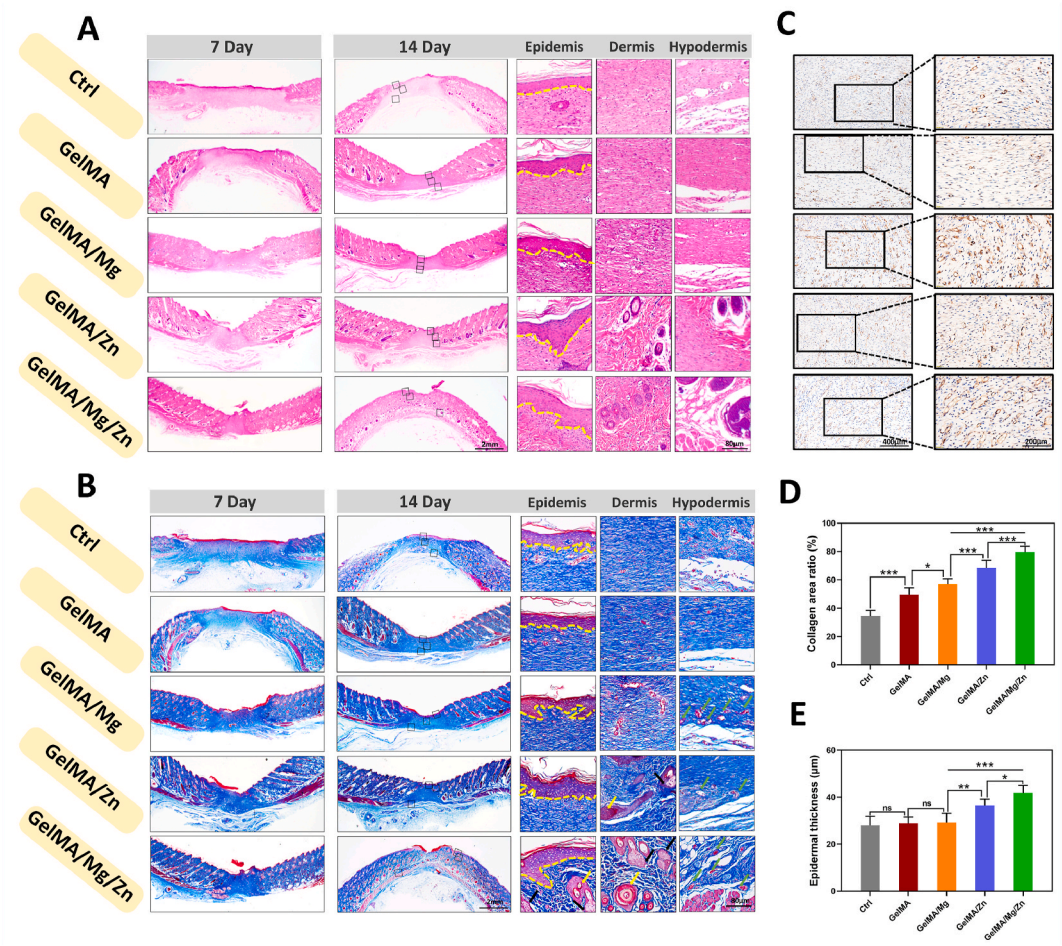

Fig. 6. *In vivo* histological evaluation of wound healing of full-thickness skin defects in rats. (A, B) Optical images and corresponding amplified images of hematoxylin–eosin and Masson staining of wounds treated with GelMA, GelMA/Mg, GelMA/Zn, and GelMA/Mg/Zn at 7 and 14 days. Yellow dotted lines indicate the boundary between the epidermis and dermis (yellow arrow: hair follicle; green arrow: blood vessel; black arrow: sebaceous gland). (C) CD31 immunohistochemical (IHC) staining results at 7 days. (D) Collagen area ratio of each group according to Masson staining done 14 days after operation. (E) Statistical chart of the epidermal thickness of the five groups. (F) CD31 IHC staining at 14 days. Data are shown as the mean ± standard deviation (n = 8). $^{*}p < 0.05$, $^{**}p < 0.01$, $^{***}p < 0.001$, ns: not significant.

Statistical analysis of the collagen content of wound skin tissue confirmed that the wound healing of the GelMA/Mg/Zn group was significantly better than that of the other groups (Fig. 6C). The degree of re-epithelialization was considered an appropriate evaluation criterion for wound repair. Fig. 6D shows that the thickness of the epidermis was smallest in the Ctrl group (28.03 ± 3.57 μm) and largest in the GelMA/Mg/Zn group (41.80 ± 3.22 μm). CD31 IHC staining was used to identify newly formed blood vessels at the skin wound. The GelMA/Mg and GelMA/Mg/Zn groups had the most CD31-positive microvessels (Fig. 6G), suggesting that the addition of Mg particles promoted vascular regeneration at the skin wound site.

The above results indicate that GelMA/Mg/Zn can promote the re-epithelialization of skin wounds in rats, promote collagen generation and maturation, and promote vascular and skin appendage regeneration. GelMA/Mg/Zn was the treatment most conducive to wound healing. In addition, histological analysis of the rat's major organs (heart, liver, spleen, lungs, and kidneys) on day 14 after treatment showed no abnormal effects or damage (Fig. S3).

3.5. GelMA/Mg/Zn hydrogel improves wound healing via STAT3 signaling pathway

To elucidate the mechanism of GelMA/Mg/Zn hydrogel promoted soft tissue wound healing, we used high-throughput RNA-Seq to study the effect of GelMA/Mg/Zn on gene expression in HSFs. Fig. 7A is the volcano map of the transcriptome sequencing results. In this study, differentially expressed genes were classified as log 2 × (fold change) > 1.00 and $p < 0.05$. There were 93 upregulated and 421 downregulated genes in the GelMA/Mg/Zn group compared with the Ctrl group. Gene clustering heat maps showed that GelMA/Mg/Zn upregulated genes related to extracellular matrix formation, cell migration, and cell adhesion in HSFs (Fig. 7B). Fig. 7C shows the bubble chart of the first 20 differential gene enrichment pathways in the KEGG pathway, which include complement and coagulation cascades, IL-17 signaling, African trypanosomiasis, and JAK-STAT signaling. STAT3 plays an important role in several wound healing processes, including migration, proliferation, angiogenesis, and growth factor production [45]. Recent studies have shown that connective tissue growth factor mediates the proliferation and migration of mouse fibroblasts through the STAT3 pathway [46]. In addition, Zn^{2+}can affect the phosphorylation level of STAT proteins, although the exact mechanism is not known [47]. Among the multiple enrichment pathways, we believe that the most relevant and influential in terms of promoting the differentiation of human fibroblasts into human myofibroblasts is the STAT signaling pathway, so we subjected it to further analysis.

Western blot analysis was performed to verify whether GelMA/Mg/Zn hydrogels promoting soft tissue wound healing were related to the STAT3 signaling pathway. Fig. 7D shows that, compared with the Ctrl

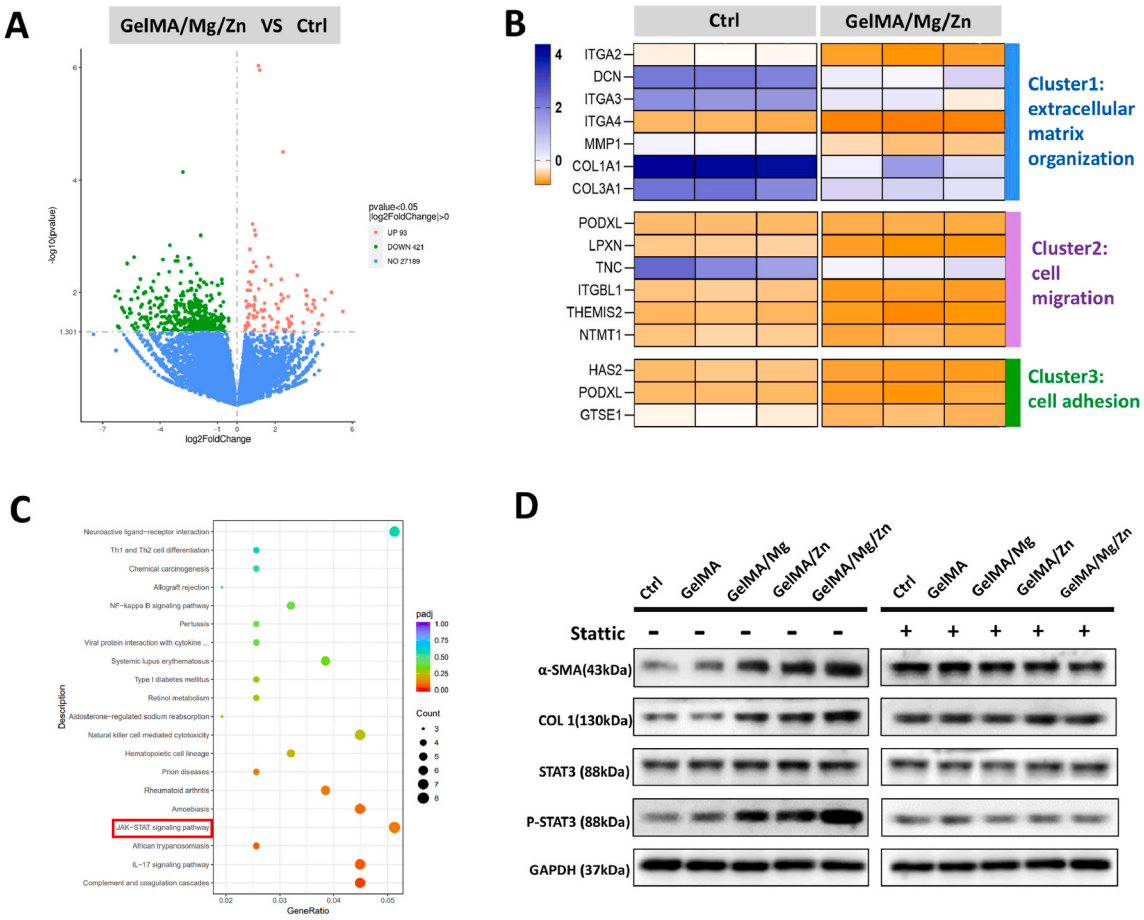

Fig. 7. Mechanism via which GelMA/Mg/Zn promotes soft tissue wound healing. (A) Volcano map showing differentially expressed genes in the control (Ctrl) and GelMA/Mg/Zn groups. (B) Hierarchical gene clustering of RNA-Seq results showing that various genes related to biological processes were different between the Ctrl and GelMA/Mg/Zn groups. (C) Representative top 20 upregulated or downregulated KEGG pathways. In the bubble diagram, the x-axis represents the enrichment score of the gene sets, the y-axis shows gene set names, and the size of the bubble indicates the number of genes in that gene set. (D) A representative Western blot shows the levels of α-SMA, COL1, STAT3, and p-STAT3 in human skin fibroblasts from the Ctrl, GelMA, GelMA/Mg, GelMA/Zn, and GelMA/Mg/Zn groups, treated and untreated with the Stattic STAT3 inhibitor.

and GelMA groups, the expression levels of p-STAT3, α-SMA and COL1 in the GelMA/Mg, GelMA/Zn, and GelMA/Mg/Zn groups significantly increased, and the gene expression levels in the GelMA/Mg/Zn group were highest among the three groups. These findings suggest that GelMA/Mg/Zn could promote the phosphorylation of STAT3, transformation of HSFs into myofibroblasts, and secretion of COL1 in activated myofibroblasts. Furthermore, these results suggest that STAT3 phosphorylation may regulate soft tissue wound healing by GelMA/Mg/Zn. To further investigate whether GelMA/Mg/Zn hydrogel promoted soft tissue wound healing is dependent on the STAT3 signaling pathway, Stattic, an inhibitor of STAT3, was used to inhibit STAT3 phosphorylation. The expression levels of P-STAT3, α-SMA, and COL1 in the five groups were consistent after Stattic addition, and were all lower than in the group without Stattic addition. Therefore, GelMA/Mg/Zn may promote the conversion of human fibroblasts into myofibroblasts by enhancing STAT3 phosphorylation to promote soft tissue wound healing.

To further verify the relationship between STAT3 phosphorylation and Zn^{2+} and Mg^{2+} release, and to explore whether Zn^{2+} and Mg^{2+} play a synergistic role and the possible mechanism, we analyzed the effects of different materials on the expression of MagT1, ZIP6, and ZIP10 and contents of Zn^{2+} and Mg^{2+} in cells. qRT-PCR confirmed that GelMA/Mg and GelMA/Mg/Zn significantly downregulated the expression of MagT1, while GelMA and GelMA/Zn had no significant effect (Fig. 8A). According to the ICP-MS results, there was no statistical difference in Mg^{2+} content in HSFs among the Ctrl, GelMA, GelMA/Mg, GelMA/Zn, and GelMA/Mg/Zn groups (Fig. 8A). In contrast, the ZIP6 and ZIP10 expression of HSFs in the GelMA/Mg/Zn and GelMA/Mg groups was significantly greater than in the Ctrl, GelMA, and GelMA/Zn groups (Fig. 8A). The intracellular level of Zn^{2+} of HSFs in the GelMA/Mg/Zn group was the highest, followed by the GelMA/Zn and GelMA/Mg groups (Fig. 8B). These results suggest that Mg^{2+} can promote Zn^{2+} entry into HSFs by up-regulating the expression of ZIP6 and ZIP10. This suggests that an increased extracellular Mg^{2+} concentration does not affect the intracellular Mg^{2+} concentration, and that the expression of MagT1 decreases when the extracellular Mg^{2+} concentration increases to maintain the intracellular Mg^{2+} concentration. Nevertheless, the presence of Mg^{2+} can upregulate the expression of ZIP6 and ZIP10, and promote the entry of more Zn^{2+} into HSFs. The increase of intracellular Zn^{2+} concentration effectively improves STAT3 phosphorylation, which promotes the expression of α-SMA, COL1, and other downstream genes, and induces the differentiation of HSFs into myofibroblasts, thus promoting the healing of skin tissue wounds (Fig. 8C).

4. Discussion

4.1. Advantages of GelMA/Mg/Zn hydrogel

The biodegradable GelMA/Mg/Zn hydrogel reported herein was constructed by low-temperature magnetic stirring and crosslinking

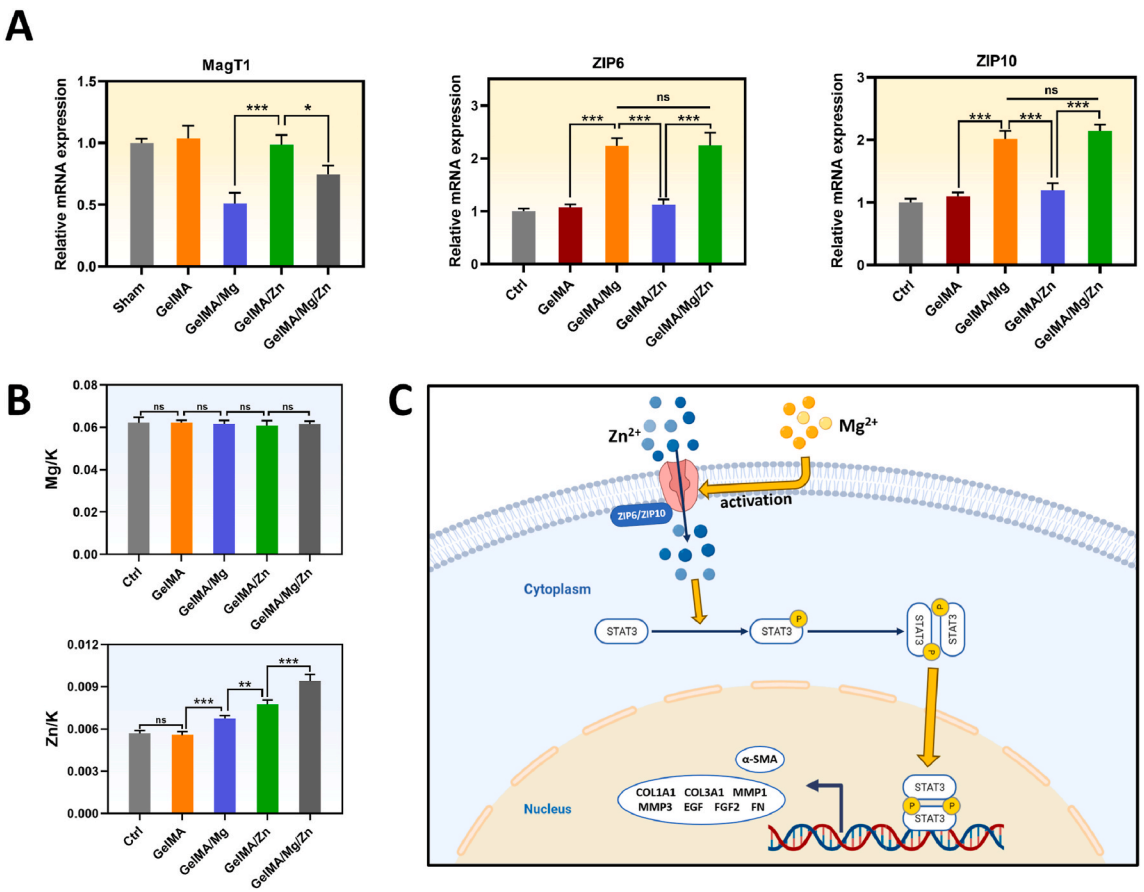

Fig. 8. Ion transport mechanism of GelMA/Mg/Zn promoting soft tissue wound healing. (A) The gene expression of MagT1, ZIP6, and ZIP10 in human skin fibroblasts from the Ctrl, GelMA, GelMA/Mg, GelMA/Zn, and GelMA/Mg/Zn groups was analyzed by RT-qPCR. (B) Total cellular Mg^{2+} and Zn^{2+} were measured by inductively coupled plasma-mass spectrometry analysis. (C) Schematic diagram of GelMA/Mg/Zn promoting human soft tissue wound healing by enhancing STAT3 phosphorylation. Data are shown as the mean ± standard deviation (n = 3). $*p < 0.05$, $**p < 0.01$, $***p < 0.001$, ns: not significant.

under 405 nm blue light, and proved to be applicable to skin wound healing *in vitro* and *in vivo*. The advantages of this hydrogel are as follows. Wide application range: GelMA hydrogel has adjustable mechanical, swelling, and degradation properties that can accommodate variations in skin strength, moisture, and wound healing speed among different types of wounds [20]. The size and proportion of Zn and Mg particles can also be adjusted. Therefore, GelMA/Mg/Zn hydrogels have promise for application in many wound types. Good biosafety: GelMA hydrogel exhibited good biocompatibility in several *in vivo* experiments [5,20]. Zinc degrades naturally in the physiological environment without producing gases and harmful products [48,49]. According to the U. S. Food and Drug Administration, Zn tolerance for adults is 40 mg/day [50]. Previous studies showed that excessive Mg^{2+} generated by the degradation of conventional Mg implants *in vivo* does not change the concentration of Mg^{2+} in serum, because Mg^{2+} will be discharged from the body through the urinary system [51,52]. Cells can tolerate concentrations of Mg^{2+} up to 16 mM (about 16-times higher than the physiological range) [53,54]. The solubility of hydrogen produced by Mg degradation is very low. In the case of well-sealed soft tissue, local air cavities may affect surrounding tissues but do not adversely affect open skin wounds [55,56]. Convenient production, storage, transportation, and preparation: in terms of the superior biomaterial properties of GelMA/Mg/Zn hydrogel and their role in promoting soft tissue wound healing, the GelMA/Mg/Zn hydrogel designed in this study is in a gel state below 4 °C and can be stored with long-term biological activity, which is conducive to large-scale production and transportation of GelMA/Mg/Zn hydrogel. Ultraviolet-light crosslinking has the advantage of being faster and more reliable than chemical and physical crosslinking methods [57]. Furthermore, the raw materials are readily obtained, the preparation method is facile and inexpensive, and there is great potential for clinical application.

4.2. Benefits of combined application of Zn and Mg particles

To our knowledge, this is the first study of the incorporation of Zn and Mg particles into GelMA hydrogel to prepare soft tissue dressings. The Mg^{2+} and Zn^{2+} released by GelMA/Mg/Zn hydrogel have strong biological activity. In addition to their own biological activities, the combination of Zn and Mg particles has the following benefit. Firstly, Mg^{2+} promotes the transport of Zn^{2+}: Our study found that the intracellular Mg^{2+} concentration was not affected by extracellular Mg^{2+} and Zn^{2+} concentration changes. The expression of MagT1 in HSFs was downregulated in the GelMA/Mg and GelMA/Zn/Mg groups, suggesting that the high concentration of extracellular Mg^{2+} maintained the same intracellular Mg^{2+} content by downregulating MagT1. Mammalian cells have a strong intracellular Mg^{2+} stabilization mechanism, maintaining intracellular Mg^{2+} within a narrow range (17–20 mM) [58,59]. The intracellular Mg^{2+} concentration fluctuates much less in response to extracellular stimulation [60,61]. In mammalian epithelial cells, low and high extracellular Mg^{2+} concentrations regulate the expression of Mg transporters to maintain a constant intracellular Mg^{2+} concentration [62]. Moreover, Mg^{2+} released by GelMA/Mg and GelMA/Mg/Zn hydrogels upregulated the expression of ZIP6 and ZIP10, and the content of Zn^{2+} in HSFs in the GelMA/Mg/Zn group was higher than that in the GelMA/Zn group. These results suggest that Mg^{2+} promotes the entry of more Zn^{2+} into HSFs through ZIP6 and ZIP10, thus effectively

enhancing STAT3 phosphorylation and inducing HSFs to differentiate into myofibroblasts. Similarly, Yu et al. co-implanted Zn/Mg ions into titanium (Zn/Mg-PIII) via plasma immersion ion implantation; the results suggested that there may be a synergistic effect between Zn and Mg. They also found that Zn^{2+} did not affect the absorption of Mg^{2+}, while Mg^{2+} increased the concentration of Zn^{2+} in rBMSCs, similar to our study [35]. Secondly, improve biocompatibility: The CCK-8 results showed that GelMA/Mg and GelMA/Zn extracts slightly affected the proliferation of HSFs and HaCats, while GelMA/Mg/Zn extracts did not. Moreover, HSFs on GelMA/Mg/Zn had better cell elongation than on GelMA/Mg and GelMA/Zn. So the biocompatibility of GelMA/Mg/Zn was better than that of GelMA/Mg and GelMA/Zn, which is also one of the advantages of the combination of Zn and Mg. This indicates that the combination of 1.25 wt% Mg and Zn particles achieved stronger biological activity. Thirdly, enhanced swelling properties of the hydrogel: the swelling rate of GelMA/Mg/Zn hydrogel was higher than that of GelMA/Zn hydrogel, which promoted the absorption of wound exudates. This is due to the hydrogen produced during the degradation of Mg particles, resulting in more pores in GelMA/Mg/Zn hydrogel.

4.3. The concentration of zinc and magnesium ions released

Mg and Zn particles react with water to form degradation products in situ, and soluble Mg^{2+} and Zn^{2+} can be transported in the hydrogel network and continuously released into the surrounding physiological environment. We believe that the concentrations of Zn^{2+} and Mg^{2+} greatly depend on particle size and the amounts of Zn and Mg particles added. Against this background, we referred to some studies concerning the effects of Zn^{2+} and Mg^{2+} on cell activity and migration promotion ability. Li et al. found that ZnPB-3, which released about 1.116 ppm (5.42 μmol/L) of Zn^{2+}, significantly promoted collagen deposition in mouse embryonic fibroblasts and inhibited inflammatory factors [63]. In addition, other studies have shown that low concentrations of Zn^{2+} (16, 20, 40, and 80 μmol/L) can promote cell proliferation and migration [64,65]. According to previous studies, Mg^{2+} affects both cell migration and adhesion in a dose dependent manner [66]. In addition, Mg^{2+} modulated the migration capacity of human umbilical vein endothelial cells, and reached a peak at 100 μmol/L [67]. We found that 1 and 10 μmol/L $ZnSO_4$ salt solution best-promoted HSF migration, while 100 μmol/L and 1 mmol/L $MgCl_2$ solutions significantly promoted HSF migration through the cell scratch assay. The effective concentrations of Zn^{2+} and Mg^{2+} in some literatures are different from those obtained in our scratch experiment, which may be due to the different cell types and culture conditions.

4.4. Relationship between the STAT3 signaling pathway and soft tissue healing

We found that increased Zn^{2+} in HSFs effectively enhanced STAT3 phosphorylation and induced HSFs differentiation into myofibroblasts, thus promoting the healing of soft tissue defect. JAK-STAT is one of the most important signaling pathways in wound healing cells; it is involved in cell proliferation and differentiation, immune regulation, and the inflammatory response [68]. STAT3 plays an important role in several wound healing processes, including migration, proliferation, angiogenesis, and the production of growth factors [45]. Recent studies have shown that connective tissue growth factor mediates the proliferation and migration of mouse fibroblasts through the STAT3 signaling pathway [47]. Several studies have shown that STAT3 can be regulated by Zn. Yang et al. found that Zn^{2+} promoted the neural differentiation of pluripotent stem cells by regulating ERK1/2 phosphorylation and STAT3 phosphorylation [44]. However, they detected few Zn-regulated molecules, and the specific mechanism through which Zn regulated neural differentiation needs to be further studied. In addition, Zn^{2+} increases mitochondrial STAT3 phosphorylation at Ser727 through the ERK pathway, thereby improving cardiac oxidative phosphorylation and inducing active astrocyte proliferation [69,70].

In summary, our results indicate that GelMA/Mg/Zn hydrogel can release Zn^{2+} and Mg^{2+}, induce HSFs differentiation into myofibroblasts, and accelerate extracellular matrix deposition through the STAT3 signaling pathway. By exploiting these features, GelMA/Mg/Zn hydrogel treatment can accelerate full-thickness defect healing and promote wound re-epithelialization and angiogenesis in rats, which provides a new theoretical and experimental basis for wound healing. Although GelMA/Zn/Mg hydrogel as a wound dressing has significant benefits *in vitro* and *in vivo*, the adhesion property needs to be improved in future experiments.

5. Conclusion

We developed a photocured biodegradable GelMA/Mg/Zn hydrogel that can be applied for skin wound healing. During the degradation of GelMA/Mg/Zn hydrogel, Mg^{2+} and Zn^{2+} with strong biological activity were produced. Magnesium ions upregulated the expressions of ZIP6 and ZIP10, and promoted Zn^{2+} entry into HSFs. An increased intracellular Zn^{2+} concentration effectively promoted STAT3 phosphorylation, thus inducing HSFs differentiation into myofibroblasts, accelerating extracellular matrix deposition, and promoting the healing of full-thickness skin defects in rats. In addition, GelMA/Mg/Zn hydrogel can promote wound re-epithelialization and angiogenesis, whose effect on wound healing is multilevel and multichannel. GelMA/Zn/Mg hydrogel shows great potential for clinical application due to its excellent biocompatible properties and ability to promote wound healing.

Data and materials availability

The data that support the findings of this study are available in the supplementary material of this article. Additional data related to this paper may be requested from the authors.

Ethics approval and consent to participate

Animal experiments were performed in accordance with the guidelines for the care and use of laboratory animals in Peking University Health Science Center (Approval No. LA 2019019). All animal experiments complied with institutional and Chinese government guidelines for the care and use of experimental animals.

CRediT authorship contribution statement

Fan Yang: Conceptualization, Methodology, Investigation, Writing – original draft. **Yijia Xue:** Methodology, Data curation, Writing – review & editing. **Feilong Wang:** Investigation, Software, Resources. **Danni Guo:** Software, Writing-review. **Yunjiao He:** Methodology. **Xiao Zhao:** Software, Writing – review & editing. **Fanyu Yan:** Software. **Yuqian Xu:** Data curation, Validation. **Dandan Xia:** Investigation, Writing – review & editing, Supervision. **Yunsong Liu:** Methodology, Writing – review & editing, Supervision.

Declaration of competing interest

The authors declare that they have no known competing financial interests or personal relationships that could have appeared to influence the work reported in this paper.

Acknowledgements

This study was supported by the National Key R&D Program of China [grant number 2021YFC2400700], the National Natural Science Foundation of China [grant numbers 82170929, 81970908]. Beijing Natural Science Foundation-Haidian Original Innovation Joint Fund Project [grant numbers L222090, L212014], and the Beijing Nova Program.

Appendix A. Supplementary data

Supplementary data to this article can be found online at https://doi.org/10.1016/j.bioactmat.2023.02.019.

References

[1] A.K. Dąbrowska, F. Spano, S. Derler, C. Adlhart, N.D. Spencer, R.M. Rossi, The relationship between skin function, barrier properties, and body-dependent factors, Skin Res. Technol. 24 (2018) 165–174, https://doi.org/10.1111/srt.12424.

[2] R.G. Frykberg, J. Banks, Challenges in the treatment of chronic wounds, Adv. Wound Care 4 (2015) 560–582, https://doi.org/10.1089/wound.2015.0635.

[3] U.H. Ko, J. Choi, J. Choung, S. Moon, J.H. Shin, Physicochemically tuned myofibroblasts for wound healing strategy, Sci. Rep. 9 (2019), 16070, https://doi.org/10.1038/s41598-019-52523-9.

[4] Y. Liang, J. He, B. Guo, Functional hydrogels as wound dressing to enhance wound healing, ACS Nano 15 (2021) 12687–12722, https://doi.org/10.1021/acsnano.1c04206.

[5] S.R. Beanes, C. Dang, C. Soo, K. Ting, Skin repair and scar formation: the central role of TGF-beta, Expet Rev. Mol. Med. 5 (2003) 1–22, https://doi.org/10.1017/s1462399403005817.

[6] G.C. Gurtner, S. Werner, Y. Barrandon, M.T. Longaker, Wound repair and regeneration, Nature 453 (2008) 314–321, https://doi.org/10.1038/nature07039.

[7] H. Hu, F.J. Xu, Rational design and latest advances of polysaccharide-based hydrogels for wound healing, Biomater. Sci. 8 (2020) 2084–2101, https://doi.org/10.1039/d0bm00055h.

[8] D. Simões, S.P. Miguel, M.P. Ribeiro, P. Coutinho, A.G. Mendonça, I.J. Correia, Recent advances on antimicrobial wound dressing: a review, Eur. J. Pharm. Biopharm. 127 (2018) 130–141, https://doi.org/10.1016/j.ejpb.2018.02.022.

[9] Q. Zeng, X. Qi, G. Shi, M. Zhang, H. Haick, Wound dressing: from nanomaterials to diagnostic dressings and healing evaluations, ACS Nano 16 (2022) 1708–1733, https://doi.org/10.1021/acsnano.1c08411.

[10] H. Dong, L. Wang, L. Du, X. Wang, Q. Li, X. Wang, J. Zhang, J. Nie, G. Ma, Smart polycationic hydrogel dressing for dynamic wound healing, Small 18 (2022), e2201620, https://doi.org/10.1002/smll.202201620.

[11] M. Farokhi, F. Mottaghitalab, M. Babaluei, Y. Mojarab, S.C. Kundu, Advanced multifunctional wound dressing hydrogels as Drug carriers, Macromol. Biosci. 22 (2022), e2200111, https://doi.org/10.1002/mabi.202200111.

[12] M. Madaghiele, C. Demitri, A. Sannino, L. Ambrosio, Polymeric hydrogels for burn wound care: advanced skin wound dressings and regenerative templates, Burns Trauma 2 (2014) 153–161, https://doi.org/10.4103/2321-3868.143616.

[13] H. Bi, H. Li, C. Zhang, Y. Mao, F. Nie, Y. Xing, W. Sha, X. Wang, D.M. Irwin, H. Tan, Stromal vascular fraction promotes migration of fibroblasts and angiogenesis through regulation of extracellular matrix in the skin wound healing process, Stem Cell Res. Ther. 10 (2019) 302, https://doi.org/10.1186/s13287-019-1415-6.

[14] E.M. Ahmed, Hydrogel: preparation, characterization, and applications: a review, J. Adv. Res. 6 (2015) 105–121, https://doi.org/10.1016/j.jare.2013.07.006.

[15] K. Dhaliwal, N. Lopez, Hydrogel dressings and their application in burn wound care, Br. J. Community Nurs. 23 (2018) S24–s27, https://doi.org/10.12968/bjcn.2018.23.Sup9.S24.

[16] J. Koehler, F.P. Brandl, A.M. Goepferich, Hydrogel wound dressings for bioactive treatment of acute and chronic wounds, Eur. Polym. J. 100 (2018) 1–11, https://doi.org/10.1016/j.eurpolymj.2017.12.046.

[17] J. Su, J. Li, J. Liang, K. Zhang, J. Li, Hydrogel preparation methods and biomaterials for wound dressing, Life 11 (2021), https://doi.org/10.3390/life11101016.

[18] B. Tao, C. Lin, X. Qin, Y. Yu, A. Guo, K. Li, H. Tian, W. Yi, D. Lei, Y. Chen, L. Chen, Fabrication of gelatin-based and Zn(2+)-incorporated composite hydrogel for accelerated infected wound healing, Mater. Today Biol. 13 (2022), 100216, https://doi.org/10.1016/j.mtbio.2022.100216.

[19] Z. Zhao, G. Li, H. Ruan, K. Chen, Z. Cai, G. Lu, R. Li, L. Deng, M. Cai, W. Cui, Capturing magnesium ions via microfluidic hydrogel microspheres for promoting cancellous bone regeneration, ACS Nano 15 (2021) 13041–13054, https://doi.org/10.1021/acsnano.1c02147.

[20] A.T. Young, O.C. White, M.A. Daniele, Rheological properties of coordinated physical gelation and chemical crosslinking in gelatin methacryloyl (GelMA) hydrogels, Macromol. Biosci. 20 (2020), e2000183, https://doi.org/10.1002/mabi.202000183.

[21] K. Yue, G. Trujillo-de Santiago, M.M. Alvarez, A. Tamayol, N. Annabi, A. Khademhosseini, Synthesis, properties, and biomedical applications of gelatin methacryloyl (GelMA) hydrogels, Biomaterials 73 (2015) 254–271, https://doi.org/10.1016/j.biomaterials.2015.08.045.

[22] S.R.U. Rehman, R. Augustine, A.A. Zahid, R. Ahmed, M. Tariq, A. Hasan, Reduced graphene oxide incorporated GelMA hydrogel promotes angiogenesis for wound healing applications, Int. J. Nanomed. 14 (2019) 9603–9617, https://doi.org/10.2147/ijn.S218120.

[23] M. Yuan, K. Liu, T. Jiang, S. Li, J. Chen, Z. Wu, W. Li, R. Tan, W. Wei, X. Yang, H. Dai, Z. Chen, GelMA/PEGDA microneedles patch loaded with HUVECs-derived exosomes and Tazarotene promote diabetic wound healing, J. Nanobiotechnol. 20 (2022) 147, https://doi.org/10.1186/s12951-022-01354-4.

[24] P.H. Lin, M. Sermersheim, H. Li, P.H.U. Lee, S.M. Steinberg, J. Ma, Zinc in wound healing modulation, Nutrients 10 (2017) 16, https://doi.org/10.3390/nu10010016.

[25] K.A. Taylor, N. Pugh, The contribution of zinc to platelet behaviour during haemostasis and thrombosis, Metallomics 8 (2016) 144–155, https://doi.org/10.1039/c5mt00251f.

[26] D. Xia, F. Yang, Y. Zheng, Y. Liu, Y. Zhou, Research status of biodegradable metals designed for oral and maxillofacial applications: a review, Bioact. Mater. 6 (2021) 4186–4208, https://doi.org/10.1016/j.bioactmat.2021.01.011.

[27] S. Yao, J. Chi, Y. Wang, Y. Zhao, Y. Luo, Y. Wang, Zn-MOF encapsulated antibacterial and degradable microneedles array for promoting wound healing, Adv. Healthc. Mater. 10 (2021), e2100056, https://doi.org/10.1002/adhm.202100056.

[28] B. Gawronska-Kozak, Scarless skin wound healing in FOXN1 deficient (nude) mice is associated with distinctive matrix metalloproteinase expression, Matrix Biol. 30 (2011) 290–300, https://doi.org/10.1016/j.matbio.2011.04.004.

[29] R. Amberg, A. Elad, D. Rothamel, T. Fienitz, G. Szakacs, S. Heilmann, F. Witte, Design of a migration assay for human gingival fibroblasts on biodegradable magnesium surfaces, Acta Biomater. 79 (2018) 158–167, https://doi.org/10.1016/j.actbio.2018.08.034.

[30] T.S. Lange, A.K. Bielinsky, K. Kirchberg, I. Bank, K. Herrmann, T. Krieg, K. Scharffetter-Kochanek, Mg^{2+} and Ca^{2+} differentially regulate beta 1 integrin-mediated adhesion of dermal fibroblasts and keratinocytes to various extracellular matrix proteins, Exp. Cell Res. 214 (1994) 381–388, https://doi.org/10.1006/excr.1994.1271.

[31] Y.W. Chen, T.T. Hsu, K. Wang, M.Y. Shie, Preparation of the fast setting and degrading Ca-Si-Mg cement with both odontogenesis and angiogenesis differentiation of human periodontal ligament cells, Mater. Sci. Eng. C Mater. Biol. Appl. 60 (2016) 374–383, https://doi.org/10.1016/j.msec.2015.11.064.

[32] S. Cheng, D. Zhang, M. Li, X. Liu, Y. Zhang, S. Qian, F. Peng, Osteogenesis, angiogenesis and immune response of Mg-Al layered double hydroxide coating on pure Mg, Bioact. Mater. 6 (2021) 91–105, https://doi.org/10.1016/j.bioactmat.2020.07.014.

[33] L. Cui, J. Liang, H. Liu, K. Zhang, J. Li, Nanomaterials for angiogenesis in skin tissue engineering, Tissue Eng. B Rev. 26 (2020) 203–216, https://doi.org/10.1089/ten.TEB.2019.0337.

[34] Q. Wu, S. Xu, F. Wang, B. He, X. Wang, Y. Sun, C. Ning, K. Dai, Double-edged effects caused by magnesium ions and alkaline environment regulate bioactivities of magnesium-incorporated silicocarnotite in vitro, Regen. Biomater. 8 (2021), rbab016, https://doi.org/10.1093/rb/rbab016.

[35] Y. Yu, G. Jin, Y. Xue, D. Wang, X. Liu, J. Sun, Multifunctions of dual Zn/Mg ion co-implanted titanium on osteogenesis, angiogenesis and bacteria inhibition for dental implants, Acta Biomater. 49 (2017) 590–603, https://doi.org/10.1016/j.actbio.2016.11.067.

[36] C.M. Cleetus, F. Alvarez Primo, G. Fregoso, N. Lalitha Raveendran, J.C. Noveron, C. T. Spencer, C.V. Ramana, B. Joddar, Alginate hydrogels with embedded ZnO nanoparticles for wound healing therapy, Int. J. Nanomed. 15 (2020) 5097–5111, https://doi.org/10.2147/ijn.S255937.

[37] Z. Guo, Z. Zhang, N. Zhang, W. Gao, J. Li, Y. Pu, B. He, J. Xie, A Mg2+/polydopamine composite hydrogel for the acceleration of infected wound healing, Bioact. Mater. 15 (2022) 203–213, https://doi.org/10.1016/j.bioactmat.2021.11.036.

[38] D. Luong, A.A. Yergeshov, M. Zoughaib, F.R. Sadykova, B.I. Gareev, I.N. Savina, T. I. Abdullin, Transition metal-doped cryogels as bioactive materials for wound healing applications, Mater. Sci. Eng. C Mater. Biol. Appl. 103 (2019), 109759, https://doi.org/10.1016/j.msec.2019.109759.

[39] B. Tao, C. Lin, X. Qin, Y. Yu, A. Guo, K. Li, H. Tian, W. Yi, D. Lei, Y. Chen, L. Chen, Fabrication of gelatin-based and Zn2+-incorporated composite hydrogel for accelerated infected wound healing, Mater. Today Bio. 13 (2022), 100216, https://doi.org/10.1016/j.mtbio.2022.100216.

[40] J. Yin, P. Xu, K. Wu, H. Zhou, X. Lin, L. Tan, H. Yang, K. Yang, L. Yang, Macroporous and antibacterial hydrogels enabled by incorporation of Mg-Cu alloy particles for accelerating skin wound healing, Acta Metall. Sin. 35 (2022) 853–866, https://doi.org/10.1007/s40195-021-01335-w.

[41] X. Zhao, Q. Lang, L. Yildirimer, Z.Y. Lin, W. Cui, N. Annabi, K.W. Ng, M. R. Dokmeci, A.M. Ghaemmaghami, A. Khademhosseini, Photocrosslinkable gelatin hydrogel for epidermal tissue engineering, Adv. Healthc. Mater. 5 (2016) 108–118, https://doi.org/10.1002/adhm.201500005.

[42] M. Zhu, Y. Wang, G. Ferracci, J. Zheng, N.J. Cho, B.H. Lee, Gelatin methacryloyl and its hydrogels with an exceptional degree of controllability and batch-to-batch consistency, Sci. Rep. 9 (2019) 6863, https://doi.org/10.1038/s41598-019-42186-x.

[43] I.M. El-Sherbiny, M.H. Yacoub, Hydrogel scaffolds for tissue engineering: progress and challenges, Glob. Cardiol. Sci Pract. 2013 (2013) 316–342, https://doi.org/10.5339/gcsp.2013.38.

[44] R.C. de Oliveira, Wilson S.E. Fibrocytes, Wound healing, and corneal fibrosis, Invest. Ophthalmol. Vis. Sci. 61 (2020) 28, https://doi.org/10.1167/iovs.61.2.28.

[45] S. Sano, K.S. Chan, J. DiGiovanni, Impact of Stat3 activation upon skin biology: a dichotomy of its role between homeostasis and diseases, J. Dermatol. Sci. 50 (2008) 1–14, https://doi.org/10.1016/j.jdermsci.2007.05.016.

[46] S.M. Zhang, C.Y. Wei, Q. Wang, L. Wang, L. Lu, F.Z. Qi, M2-polarized macrophages mediate wound healing by regulating connective tissue growth factor via AKT, ERK1/2, and STAT3 signaling pathways, Mol. Biol. Rep. 48 (2021) 6443–6456, https://doi.org/10.1007/s11033-021-06646-w.

[47] M. Yang, D. Bao, A. Shi, H. Yuan, J. Wang, W. He, X. Tong, H. Qin, Zinc promotes patient-derived induced pluripotent stem cell neural differentiation via ERK-STAT signaling, Stem Cell. Dev. 29 (2020) 863–875, https://doi.org/10.1089/scd.2020.0016.

[48] Y. Su, H. Yang, J. Gao, Y.X. Qin, Y. Zheng, D. Zhu, Interfacial zinc phosphate is the key to controlling biocompatibility of metallic zinc implants, Adv. Sci. 6 (2019), 1900112, https://doi.org/10.1002/advs.201900112.
[49] Y.F. Zheng, X.N. Gu, F. Witte, Biodegradable metals, Mater. Sci. Eng.: R. Rep. 77 (2014) 1–34, https://doi.org/10.1016/j.mser.2014.01.001.
[50] C. Livingstone, Zinc: physiology, deficiency, and parenteral nutrition, Nutr. Clin. Pract. 30 (2015) 371–382, https://doi.org/10.1177/0884533615570376.
[51] J. Draxler, E. Martinelli, A.M. Weinberg, A. Zitek, J. Irrgeher, M. Meischel, S. E. Stanzl-Tschegg, B. Mingler, T. Prohaska, The potential of isotopically enriched magnesium to study bone implant degradation in vivo, Acta Biomater. 51 (2017) 526–536, https://doi.org/10.1016/j.actbio.2017.01.054.
[52] E. Zhang, L. Xu, G. Yu, F. Pan, K. Yang, In vivo evaluation of biodegradable magnesium alloy bone implant in the first 6 months implantation, J. Biomed. Mater. Res. 90 (2009) 882–893, https://doi.org/10.1002/jbm.a.32132.
[53] R. Karunakaran, S. Ortgies, A. Tamayol, F. Bobaru, M.P. Sealy, Additive manufacturing of magnesium alloys, Bioact. Mater. 5 (2020) 44–54, https://doi.org/10.1016/j.bioactmat.2019.12.004.
[54] D. Maradze, D. Musson, Y. Zheng, J. Cornish, M. Lewis, Y. Liu, High magnesium corrosion rate has an effect on osteoclast and mesenchymal stem cell role during bone remodelling, Sci. Rep. 8 (2018), 10003, https://doi.org/10.1038/s41598-018-28476-w.
[55] T. Kraus, S.F. Fischerauer, A.C. Hänzi, P.J. Uggowitzer, J.F. Löffler, A.M. Weinberg, Magnesium alloys for temporary implants in osteosynthesis: in vivo studies of their degradation and interaction with bone, Acta Biomater. 8 (2012) 1230–1238, https://doi.org/10.1016/j.actbio.2011.11.008.
[56] D. Persaud-Sharma, A. McGoron, Biodegradable magnesium alloys: a review of material development and applications, J. Biomim. Biomater. Tissue Eng. 12 (2012) 25–39. https://doi.org/10.4028/www.scientific.net/JBBTE.12.25.
[57] G. Eke, N. Mangir, N. Hasirci, S. MacNeil, V. Hasirci, Development of a UV crosslinked biodegradable hydrogel containing adipose derived stem cells to promote vascularization for skin wounds and tissue engineering, Biomaterials 129 (2017) 188–198, https://doi.org/10.1016/j.biomaterials.2017.03.021.
[58] R.D. Grubbs, Intracellular magnesium and magnesium buffering, Biometals 15 (2002) 251–259, https://doi.org/10.1023/a:1016026831789.
[59] A.M. Romani, Magnesium homeostasis in Mammalian cells, Met. Ions Life Sci. 12 (2013) 69–118, https://doi.org/10.1007/978-94-007-5561-14.
[60] A. Goytain, G.A. Quamme, Identification and characterization of a novel mammalian Mg2+ transporter with channel-like properties, BMC Genom. 6 (2005) 48, https://doi.org/10.1186/1471-2164-6-48.
[61] H. Zhou, Clapham D. E. Mammalian MagT1 and TUSC3 are required for cellular magnesium uptake and vertebrate embryonic development, Proc. Natl. Acad. Sci. U. S. A. 106 (2009) 15750–15755, https://doi.org/10.1073/pnas.0908332106.
[62] F.I. Wolf, V. Trapani, M. Simonacci, L. Mastrototaro, A. Cittadini, M. Schweigel, Modulation of TRPM6 and Na(+)/Mg(2+) exchange in mammary epithelial cells in response to variations of magnesium availability, J. Cell. Physiol. 222 (2010) 374–381, https://doi.org/10.1002/jcp.21961.
[63] J. Li, X. Liu, L. Tan, Z. Cui, X. Yang, Y. Liang, Z. Li, S. Zhu, Y. Zheng, K.W.K. Yeung, X. Wang, S. Wu, Zinc-doped Prussian blue enhances photothermal clearance of Staphylococcus aureus and promotes tissue repair in infected wounds, Nat. Commun. 10 (2019) 4490, https://doi.org/10.1038/s41467-019-12429-6.
[64] P. Bao, H.Y. Liu, Y.Q. Wang, Y.J. Tan, L.F. Li, C.X. Xu, L. Huang, X.H. Zhao, [Effects of zinc ions on biological functions of human umbilical vein endothelial cells], Zhonghua Xinxueguanbing Zazhi 46 (2018) 390–395, https://doi.org/10.3760/cma.j.issn.0253-3758.2018.05.012.
[65] M. Tyszka-Czochara, P. Paśko, W. Reczyński, M. Szlósarczyk, B. Bystrowska, W. Opoka, Zinc and propolis reduces cytotoxicity and proliferation in skin fibroblast cell culture: total polyphenol content and antioxidant capacity of propolis, Biol. Trace Elem. Res. 160 (2014) 123–131, https://doi.org/10.1007/s12011-014-0019-3.
[66] R. Amberg, A. Elad, F. Beuer, C. Vogt, J. Bode, F. Witte, Effect of physical cues of altered extract media from biodegradable magnesium implants on human gingival fibroblasts, Acta Biomater. 98 (2019) 186–195, https://doi.org/10.1016/j.actbio.2019.07.022.
[67] K.A. Lapidos, E.C. Woodhouse, E.C. Kohn, L. Masiero, Mg^{2+}-induced endothelial cell migration: substratum selectivity and receptor-involvement, Angiogenesis 4 (2001) 21–28, https://doi.org/10.1023/a:1016619414817.
[68] S.W. Jere, H. Abrahamse, N.N. Houreld, The JAK/STAT signaling pathway and photobiomodulation in chronic wound healing, Cytokine Growth Factor Rev. 38 (2017) 73–79, https://doi.org/10.1016/j.cytogfr. 2017. 10.001.
[69] Z. Huiliang, Y. Mengzhe, W. Xiaochuan, W. Hui, D. Min, W. Mengqi, W. Jianzhi, C. Zhongshan, P. Caixia, L. Rong, Zinc induces reactive astrogliosis through ERK-dependent activation of Stat3 and promotes synaptic degeneration, J. Neurochem. 159 (2021) 1016–1027, https://doi.org/10.1111/jnc.15531.
[70] G. Zhang, M. Sheng, J. Wang, T. Teng, Y. Sun, Q. Yang, Z. Xu, Zinc improves mitochondrial respiratory function and prevents mitochondrial ROS generation at reperfusion by phosphorylating STAT3 at Ser (727), J. Mol. Cell. Cardiol. 118 (2018) 169–182, https://doi.org/10.1016/j.yjmcc.2018.03.019.